Strojniški vestnik - Journal of Mechanical Engineering 55(2009)6, 369-380
UDC 621.22
Paper received: 22.12.2008
Paper accepted: 08.07.2009

A Novel Pelton Turbine Model for Water Hammer Analysis

Uroš Karadžić[1,*] - Anton Bergant[2] - Petar Vukoslavčević[1]
[1] University of Montenegro, Faculty of Mechanical Engineering, Montenegro
[2] Litostroj Power d.o.o., Slovenia

This paper presents a novel Pelton turbine model for water hammer analysis. Water hammer phenomena have been investigated in Perućica high-head hydropower plant (HPP), Montenegro. During its first phase of modernisation and refurbishment new distributors (needle valves) have been installed on the first two Pelton turbine units. Closure of the Pelton turbine distributors for the case of emergency shut-down and load rejection under governor control is modelled by two different closing laws i.e. the two-speed closing law and the law that considers actual (measured) needle stroke. Dissipation torques in turbine housing and shaft bearings are considered in the model. Stop procedure of the turbine unit is also investigated. Numerical results using the standard quasi-steady friction model and the convolution based unsteady friction model for different distributor closing laws are compared with the results of measurements. The agreement between computed and measured results is reasonable. It is shown that the effect of unsteady friction on water hammer events in Perućica HPP is of little importance (slow varying transients).

Keywords: water hammer, Pelton turbine, high-head HPP, turbine speed change, unsteady friction

0 INTRODUCTION

Water hammer control is essential to assure safe operation of hydropower plant (HPP). Excessive transient loads may disturb the overall operation of the plant and damage the system components, for example pipe rupture may occur. In hydropower plants water hammer is induced by turbine load acceptance and reduction, load rejection under governor control, emergency shut-down and unwanted runaway, and closure and opening of the safety shutoff valve. Water hammer causes pressure to rise or drop in penstocks of the hydropower plants, rotational speed change of turbine units and level variations in surge tanks [1]. The water hammer phenomenon is traditionally described by one-dimensional unsteady pipe flow equations and equations describing boundary elements (reservoir, valve, surge tank, turbine). In contrast to reaction type water turbines that are well defined in literature as boundary conditions for water hammer analysis [2] to [4], the impulse type Pelton turbine is not well defined; usually it is represented as an end-valve boundary condition [5] and [6].

This paper presents a novel Pelton turbine model for water hammer analysis that includes dynamics of the distributor (end-valve) with a jet deflector and the turbine wheel. In the first part of the paper mathematical tools for solving water hammer equations are presented. Water hammer is fully described by two hyperbolic partial differential equations, the equation of continuity and the momentum equation [3] and [4]. These equations are solved by the method of characteristics (MOC) using efficient staggered (diamond) grid [3]. Friction losses in tunnels and penstocks of hydropower plants are traditionally estimated by the quasi-steady friction model. It is clear that the role of friction in one-dimensional pipe flow depends on the system under analysis; it is important for systems that are unsteady friction dominant (i.e., unsteady friction dominates over steady friction). Unsteady friction arises from the extra losses from the two-dimensional nature of the unsteady velocity profile. It is desirable to have a model that takes into account higher dimensional velocity profile behaviour, but still can be efficiently implemented in the one-dimensional analysis. In doing so, a convolution based unsteady friction model [7] is used in this paper. Two different closing laws for the distributor (needle valve) of the Pelton turbine are investigated. Precise modelling of Pelton turbine distributor stroke is essential for accurate numerical results. A novel model for calculation of Pelton turbine rotational speed change during emergency shut-down is presented in detail. In the second part of the paper comparisons of computed and experimental results are made for turbine load rejection cases (load rejection under

*Corr. Author's Address: Faculty of Mechanical Engineering, Dzordza Vasingtona nn, 81000 Podgorica, Montenegro, uros.karadzic@ac.me

governor control, emergency shut-down) from different initial powers and for turbine unit stop from speed no-load conditions. All the presented numerical models give very good fit with results of measurements. It is shown that unsteady friction effects have a small impact on water hammer events in the Perućica HPP flow-passage system (slow varying transients).

1 THEORETICAL MODEL

Water hammer is the transmission of pressure waves along the pipeline resulting from a change in flow velocity. The simplified continuity and momentum equations, appropriate for most engineering applications, which are solved to compute the liquid unsteady pipe flow are [3] and [4],

$$\frac{\partial H}{\partial t}+\frac{a^2}{gA}\frac{\partial Q}{\partial x}=0\,, \tag{1}$$

$$\frac{\partial H}{\partial x}+\frac{1}{gA}\frac{\partial Q}{\partial t}+\frac{fQ|Q|}{2gDA^2}=0\,, \tag{2}$$

where H is piezometric head (head), Q is discharge, a is pressure wave speed, D is pipe diameter, A is pipe area, g is gravitational acceleration, f is Darcy-Weisbach friction factor, x is distance along the pipe, and t is time. For solving Eqs. (1) and (2) the staggered (diamond) grid [3] in applying the method of characteristics (MOC) is used in this paper. At a boundary (reservoir, Pelton turbine), a device-specific equation replaces one of the MOC water hammer compatibility equations.

1.1 Modelling Friction Losses

Friction losses in tunnels and penstocks of hydropower plants are usually calculated by quasi-steady friction model. This model does not give satisfactory results for fast transients when numerical results are compared with experiments [8]. The friction factor f can be expressed as the sum of the quasi-steady part f_q and the unsteady part f_u [9],

$$f = f_q + f_u\,. \tag{3}$$

The quasi-steady friction factor depends on the Reynolds number and relative pipe roughness and it is updated every time step. In this paper the Halland explicit equation [10] is used,

$$\frac{1}{f_q}=\left\{-1.8\log\left[\frac{6.9}{\mathrm{Re}}+\left(\frac{\delta}{3.7D}\right)^{1.11}\right]\right\}^2\,, \tag{4}$$

where Re is Reynolds number and δ is absolute pipe roughness. The unsteady friction factor is calculated using a convolution based model (CBM) [7]. In computationally efficient and accurate CBM the unsteady friction factor is expressed as a finite sum of N_k functions $y_k(t)$ [11],

$$f_u=\frac{32\nu A}{DQ|Q|}\sum_{k=1}^{N_k}y_k(t)\,, \tag{5}$$

with

$$y_k(t+2\Delta t)=e^{-n_kK\Delta t}\left\{\begin{matrix}e^{-n_kK\Delta t}y_k(t)+\\ m_k\left[Q(t+2\Delta t)-Q(t)\right]\end{matrix}\right\}, \tag{6}$$

where ν is kinematic viscosity, N_k is number of exponential terms ($N_{k,max}$ = 10), Δt is time step, and K is constant equal to $4\,\nu/D^2$. Coefficients m_k and n_k have been developed for Zielke's [7] and Vardy-Brown's [12] and [13] weighting functions and can be found in [11]. In addition, a momentum correction factor (β), defined by Eq. (7), is incorporated into the MOC solution when CBM model is used [14],

$$\beta=\frac{1}{AV^2}\int_A v^2\,dA\,, \tag{7}$$

where v is flow velocity. The momentum correction factor can be determined from either the log or power laws for the velocity distribution [15].

2 A NOVEL PELTON TURBINE MODEL

Pelton turbine distributor (needle valve) is utilized for control of discharge and consequently for control of the turbine output. Discharge is adjusted by closing or opening the nozzle mouth by means of a needle (Fig. 1) and with an appropriate position of the jet deflector. It should be noted that the discharge through the nozzle is solely dependent on the position of the needle; it is not dependent on the turbine speed [16]. Consequently, water hammer equations and the dynamic equation of the turbine unit rotating parts can be solved separately. In this way the instantaneous head at the nozzle inlet and the instantaneous discharge through the nozzle are calculated by the MOC algorithm and these values are used as input in the solution method

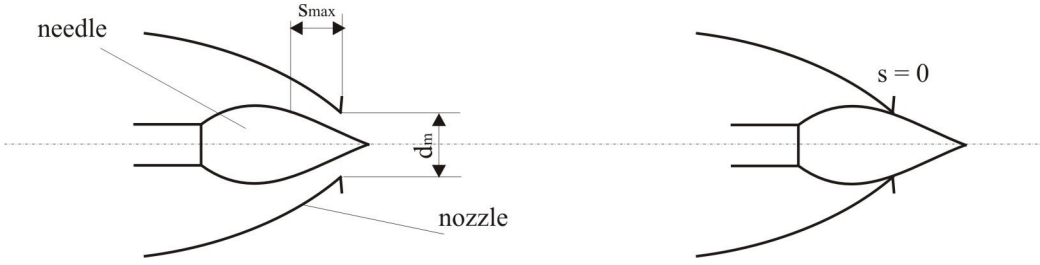

Fig. 1. *Pelton turbine distributor (needle valve)*

for the dynamic equation of the unit rotating parts.

The instantaneous discharge through the nozzle ($(Q_u)_t$) is calculated by the following equation,

$$(Q_u)_t = K_Q A_m \sqrt{2g(H_{u,t} - H_d)}\,, \tag{8}$$

where K_Q is nozzle discharge coefficient, A_m is nozzle area, $H_{u,t}$ is head at the nozzle inlet, and H_d is constant head downstream the nozzle. Typical functional dependency of the discharge coefficient K_Q and the ratio of needle stroke s and nozzle diameter d_m is depicted in Fig. 2. The needle closing law is expressed as follows,

$$s = \tau \cdot s_{\max}\,, \tag{9}$$

where τ is dimensionless nozzle opening, and s_{max} is maximum needle stroke.

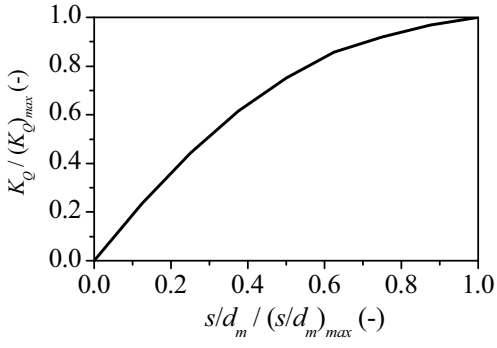

Fig. 2. *Typical discharge coefficient of Pelton turbine nozzle*

The dimensionless nozzle opening for the case of emergency shut-down of the turbine unit can be calculated using two-speed closing law [17]. A model with a two-speed closure better attenuates pressure pulses compared to the model with one-speed closure (classical linear closure). This means that at the end of the closure the needle actually moves a little bit slower (natural damping). For the time $t < t_p$ the dimensionless nozzle opening is expressed as follows,

$$\tau = \tau_i - \left(\tau_i - \tau_f\right)\left(\frac{t}{t_{c1}}\right)^{Em1}, \tag{10}$$

and for $t_p \le t \le t_c$,

$$\tau = \tau_1 - \left(\tau_1 - \tau_f\right)\left(\frac{t - t_p}{t_c - t_p}\right)^{Em2}, \tag{11}$$

where τ_i is initial opening of the nozzle, τ_f is final opening of the nozzle, τ_1 is nozzle opening at time $t = t_p$, t_p is natural damping starting time (time at the begining of the second step of the needle closure), t_c is needle closing time, t_{c1} is closure time for the one speed closure case, E_{m1}, E_{m2} are nozzle closure parameters.

For the case of load rejection under governor control the two speed closure is not employed because the needle finally stays in speed no-load position that is larger than the needle position when the second closure step begins [17]. In this case the actual (measured) needle stroke (ANS) is used.

2.1 Pelton Turbine Emergency Shut-down

The emergency shut-down of the turbine unit is the most severe normal operating transient regime [4]. The turbine is disconnected from the electrical grid followed by simultaneous gradual full-closure of the needle(s) and rapid activation of the jet deflector(s) (deflection of the jet from the wheel). The equation that describes dynamic behaviour of the Pelton turbine unit rotating parts during emergency shut-down is,

$$J\frac{d\omega}{dt} = M_h - \left(M_{fr} + M_{air}\right), \tag{12}$$

where J is polar moment of inertia of the turbine unit rotating parts, ω *is* angular velocity, M_h is hydraulic torque, M_{fr} is shaft bearing friction torque, and M_{air} is fluid damping torque

(ventilation losses in the turbine housing). A novel solution of Eq. (12) including a hydraulic brake is presented in this paper; a simplified solution of Eq. (12) that considers only the effect of jet deflector can be found in [17]. By introducing the relative speed change φ,

$$\varphi = \frac{n}{n_r} - 1 , \tag{13}$$

and the mechanical starting time T_a [1], [2] and [4],

$$T_a = \frac{\pi}{30}\frac{Jn_r}{M_r}, \tag{14}$$

into Eq. (12), after rearrangement it follows,

$$T_a \frac{d\varphi}{dt} = m_h - m_{fr} - m_{air} , \tag{15}$$

where n is turbine rotational speed (traditionally in rpm), r is rated, M_r is rated torque, and m is dimensionless torque ($m = M/M_r$).

The dimensionless hydraulic torque is expressed as follows,

$$m_h = \frac{M_h}{M_r} = \frac{1}{M_r} F_h \frac{D_k}{2}, \tag{16}$$

where F_h is jet hydraulic force [18] and [19],

$$F_h = 2\rho Q_m \left(V_m - u\right), \tag{17}$$

where u is peripheral velocity,

$$u = \frac{D_k \pi n_r}{60}\left(\varphi + 1\right), \tag{18}$$

where D_k is wheel diameter, ρ is water mass density, Q_m is discharge to the turbine wheel, and V_m is jet velocity ($V_m = Q_m / A_m$).

The discharge that acts on the turbine wheel can be evaluated from the following equation ($t \le t_{def}$) [20],

$$Q_m = Q_u \left(1 - \frac{t}{t_{def}}\right)^{0.11}, \tag{19}$$

where t_{def} is jet deflector operating time.

The dimensionless shaft bearing friction torque is [19] and [21],

$$m_{fr} = \frac{M_{fr}}{M_r} = \frac{1}{M_r}\mu_b \frac{D_b}{2}\left(R_{Ab} + R_{Bb}\right), \tag{20}$$

where D_b is shaft bearing diameter, and μ_b is shaft bearing friction coefficient. The resultant forces in the shaft bearings R_{Ab}, R_{Bb} of the horizontal-shaft unit are due to hydraulic force, weight of the wheels, weight of the shaft and weight of the generator.

The dimensionless fluid damping torque is expressed by [21],

$$m_{air} = \frac{M_{air}}{M_r} = \frac{1}{M_r} K_{air} n_r^2 \left(\varphi + 1\right)^2 , \tag{21}$$

where K_{air} is fluid (air) damping coefficient. It should be noted that complex flow phenomena in the turbine housing could be investigated by modern flow visualization techniques [22].

If we introduce expressions,

$$K_1 = \frac{\rho D_k Q_m}{M_r T_a}\left(V_m - \frac{D_k \pi n_r}{60}\right) - \\ - \frac{\mu_b D_b R_{Ab}}{M_r T_a} - \frac{K_{air} n_r^2}{M_r T_a} , \tag{22}$$

$$K_2 = -\left(\frac{\rho D_k^2 \pi n_r Q_m}{60 M_r T_a} + \frac{2K_{air} n_r^2}{M_r T_a}\right), \tag{23}$$

$$K_3 = -\frac{K_{air} n_r^2}{M_r T_a}, \tag{24}$$

then the dynamic equation reads as follows,

$$\frac{d\varphi}{dt} = K_3 \varphi^2 + K_2 \varphi + K_1 , \tag{25}$$

with the following solutions for the speed change during $t \le t_{def}$ [23],

if ($4K_1K_3 > K_2^2$) then,

$$\varphi = \frac{\sqrt{4K_1K_3 - K_2^2}}{2K_3} \tan\left[\begin{array}{l}\frac{\sqrt{4K_1K_3 - K_2^2}}{2}\left(t - t_0\right) + \\ + \tan^{-1}\left(\frac{2K_3\varphi_0 + K_2}{\sqrt{4K_1K_3 - K_2^2}}\right)\end{array}\right] - \frac{K_2}{2K_3} \tag{26}$$

if ($4K_1K_3 < K_2^2$) then

$$\varphi = \frac{p \mp q \cdot \exp\left[K_3\left(p - q\right)\left(t - t_0\right) + \ln\left|\frac{\varphi_0 - p}{\varphi_0 - q}\right|\right]}{1 \mp \exp\left[K_3\left(p - q\right)\left(t - t_0\right) + \ln\left|\frac{\varphi_0 - p}{\varphi_0 - q}\right|\right]} \tag{27}$$

where φ_0 is value of the relative speed at initial time $t = t_0$, p and q are defined as,

$$p = \frac{-K_2 + \sqrt{K_2^2 - 4K_1K_3}}{2K_3}$$
$$q = \frac{-K_2 - \sqrt{K_2^2 - 4K_1K_3}}{2K_3}. \quad (28)$$

The hydraulic torque affects the turbine wheel until the jet deflector deflects all the water into the tailrace ($t=t_{def}$). At $t > t_{def}$ the hydraulic torque is set to zero and Eqs. (26) and (27) are still valid with t_{def} and φ_{def} instead t_0 and φ_0 where φ_{def} is relative speed at $t = t_{def}$. Expressions K_i (i = 1, 2, 3) are,

$$K_1 = -\left(\frac{\mu_b D_b R_{Ab}}{M_r T_a} + \frac{K_{air} n_r^2}{M_r T_a} \right), \quad (22a)$$

$$K_2 = -\frac{2K_{air} n_r^2}{M_r T_a}, \quad (23a)$$

$$K_3 = -\frac{K_{air} n_r^2}{M_r T_a}. \quad (24a)$$

When the turbine speed drops to $n = 0.6n_r$ (standard value) a hydraulic brake is switched on; then Eq. (15) is modified to,

$$T_a \frac{d\varphi}{dt} = -m_{fr} - m_{air} - m_{hb}. \quad (29)$$

In our case study the hydraulic brake is a nozzle mounted on the opposite side of the wheel. The hydraulic brake is fed by a pipe connected to the main pipeline between the nozzle and the spherical valve. The dimensionless hydraulic brake torque is [24],

$$m_{hb} = \frac{M_{hb}}{M_r} = \frac{1}{M_r} \rho Q_{hb} \frac{D_k}{2} \cdot \left(\frac{4Q_{hb}}{\pi d_{hb}^2} + \frac{D_k \pi n_r}{60} (\varphi + 1) \right), \quad (30)$$

with hydraulic brake discharge,

$$Q_{hb} = 0.9 \frac{d_{hb}^2 \pi}{4} \sqrt{2gH_{hb}}, \quad (31)$$

where H_{hb} is available head at hydraulic brake ($H_{hb} \equiv H_u$) and d_{hb} is hydraulic brake nozzle diameter. Eqs. (26) and (27) are still valid with t_{hb} and φ_{hb} instead t_0 and φ_0. Expressions K_i (i = 1, 2, 3) are,

$$K_1 = -\frac{\rho D_k Q_{hb}}{2M_r T_a} \left(\frac{4Q_{hb}}{\pi d_{hb}^2} + \frac{D_k \pi n_r}{60} \right) - \frac{\mu_b D_b R_{Ab}}{M_r T_a} - \frac{K_{air} n_r^2}{M_r T_a}, \quad (22b)$$

$$K_2 = -\left(\frac{\rho D_k^2 \pi n_r Q_{hb}}{120 M_r T_a} + \frac{2K_{air} n_r^2}{M_r T_a} \right), \quad (23b)$$

$$K_3 = -\frac{K_{air} n_r^2}{M_r T_a}, \quad (24b)$$

where t_{hb} is hydraulic brake starting time (time when the hydraulic brake is switched on), and φ_{hb} is relative speed at $t = t_{hb}$.

2.2 Other Transient Operating Regimes

The solution method that describes dynamic behaviour of the Pelton turbine unit rotating parts during load rejection under governor control has been developed in a similar way. The turbine is disconnected from the electrical grid followed by simultaneous gradual closure of the needle(s) to the speed-no load position and controlled manouvre of the jet deflector(s) i.e. rapid activation at the first instant followed by gradual adjustment of the deflector to the speed-no load position. At the needle speed no-load position the distributor provides sufficient discharge to maintain the rated turbine rotational speed. In this case the hydraulic torque is balanced with disipation torques and the turbine speed is calculated by the following equation,

$$\varphi = \frac{-K_2 + \sqrt{K_2^2 - 4K_1K_3}}{2K_3}, \quad (32)$$

with,

$$K_1 = -\rho D_k Q_m \left(V_m - \frac{D_k \pi n_r}{60} \right) + \mu_b D_b R_{Ab} + K_{air} n_r^2, \quad (22c)$$

$$K_2 = \frac{\rho D_k^2 \pi n_r Q_m}{60} + 2K_{air} n_r^2, \quad (23c)$$

$$K_3 = K_{air} n_r^2. \quad (24c)$$

In this case all the discharge through the nozzle acts on the turbine wheel i.e. $Q_m \equiv Q_u$.

For turbine start-up the jet deflector(s) is moved from closed to its open position followed by gradual opening of the needle(s) to speed-no load position. The discharge through the nozzle(s) acts on the turbine wheel and, after some time, the hydraulic torque is balanced with dissipation torques resulting in rated turbine speed at the end of the process. The turbine is connected to the electrical grid followed by further opening of the needle(s) to the position controlled by the turbine governor.

Turbine stop procedure from the speed no-load conditions to the turbine stand-still using hydraulic brake is as follows. Needle(s) and jet deflector close from their speed no-load positions and the turbine is assumed to slow-down only by dissipation torques until the turbine speed drops to $n = 0.6n_r$ when the hydraulic brake is switched on. Now, the turbine stop becomes faster and finally the turbine is stopped ($n = 0$ min^{-1}).

3 PERUĆICA HPP FLOW-PASSAGE SYSTEM

Perućica HPP flow-passage system is a complex system comprised of an intake structure with a guard gate [25], a concrete tunnel T (length L_T = 3335 m, diameter D_T = 4.8 m), orifice type surge tank (inflow and outflow orifice head loss coefficients: ζ_{in} = 1.65 and ζ_{out} = 2.48) of cylindrical cross-section (diameter D_{ST} = 8.0 m) with an expansion at elevation z = 611.0 m (D_{ST} = 12.0 m) and overflow (elevation: z_{ov} = 628.0 m; width of the overflow weir: b_{ov} = 7.98 m with discharge coefficient μ_{ov} = 0.4) and three parallel steel penstocks with horizontal-shaft Pelton turbines built at their downstream ends (Fig. 3) [17] and [20]. The length of each penstock is about 2000 m (see Table 1 for details) whereby penstock *I* feeds two turbine units (A1 and A2) with rated unit power of 39 MW, penstock *II* feeds three turbine units (A3, A4 and A5) of 39 MW each and penstock *III* feeds two units (A6 and A7) of 59 MW each. A new turbine unit (A8) with a rated power of 59 MW is to be installed in the near future. The maximum water level at the intake is 613 m and the minimum one is 602.5 m.

The Pelton wheel diameter of units A1 to A5 is D_k = 2400 mm and for units A6 and A7 is D_k = 2100 mm. Basic characteristics of the Pelton turbine units are presented in Table 2. The turbine inlet spherical valves diameters are D_z = 1000 mm and D_z = 1200 mm, respectively. The valves are equipped with a passive actuator comprised of a hydraulic servomotor.

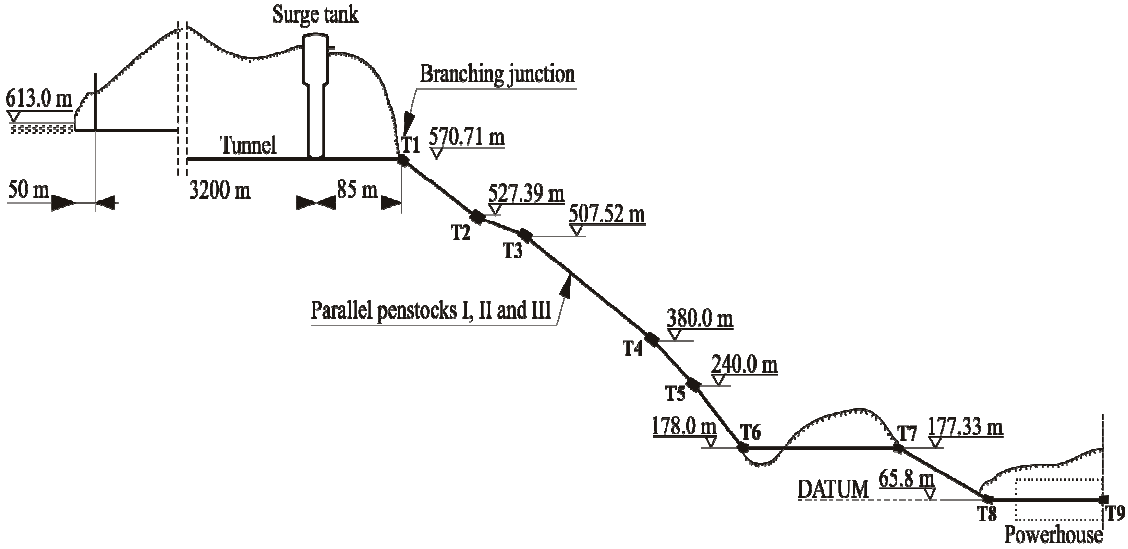

Fig. 3. *Layout of Perućica HPP*

Table 1. *Geometrical characteristics of penstocks*

Section	Length (m)	Penstock *I*		Penstock *II*		Penstock *III*	
		Pipe diameter (mm)	Pipe wall thickness (mm)	Pipe diameter (mm)	Pipe wall thickness (mm)	Pipe diameter (mm)	Pipe wall thickness (mm)
T_1-T_2	75.0	2200	10	2200	10	2650	12
T_2-T_3	61.0	2200	10	2200	10	2650	12
T_3-T_4	330.5	2200-2100	10	2200	10-16	2650	12-13
T_4-T_5	318.0	2100-2000	16-25	2200	17-23	2650	13-21
T_5-T_6	123.0	2000	26-29	2200	24-27	2650	21-24
T_6-T_7	672.0	1900	27.5	2200-2100	26	2500	23
T_7-T_8	238.0	1800	27-39	2100	26-34	2500	24-29
T_8-T_9	*I*: 53.0 *II*: 99.8 *III*: 146.6	1800	39	2100	34	2500	29

Table 2. *Characteristics of Pelton turbine units*

Turbine unit	Rated unit power (MW)	Rated net head (m)	Rated speed (min^{-1})
A1,A2,A3,A4	39	526	375
A5	39	526	375
A6,A7	59	526	428
Turbine unit	Number of runners per turbine unit	The polar moment of inertia of the unit rotating parts J (tm^2)	Number of needles per turbine runner
A1,A2,A3,A4	2	168.75	1
A5	2	168.75	1
A6,A7	2	200	2
Turbine unit	Stroke of the needle (mm)	Closing time of the needle (s)	Opening time of the needle (s)
A1,A2,A3,A4	150	85	30
A5	195	80	30
A6,A7	166	80	50

Influental quantities were continuously measured during transient operating regimes including pressure at the upstream end of the distributor, stroke of the needle, stroke of the jet deflector and turbine rotational speed. These measurements were carried out on turbine units A1 and A2. Pressures were measured by absolute high-pressure piezoelectric transducers *Cerabar T PMP 131-A1101A70 Endress + Hauser* (range 0 to 100 bar, uncertainty in measurement ±0.5%). The needle stroke and the stroke of the jet deflector were measured by discplacement transducers *Balluff BTL5-S112-M0175-B-532* and *Balluff BTL5-S112-M0275-B-532*, respectively. Uncertainty of these sensors is ±0.03 mm. The turbine rotational speed was measured using inductive sensor *Balluff BES M18MI-PSC50B-S04K* (uncertainty in measurement ±0.03%).

4 COMPARISONS OF NUMERICAL AND FIELD TEST RESULTS

During commissioning of the turbine units A1 and A2 the following regimes were investigated: the unit start-up and stop, load acceptance and reduction, load rejection under governor control and emergency shut-down, and closure of turbine safety valve against the discharge. Numerical results from the standard quasi-steady friction model (QSF) and the convolution based unsteady friction model

(CBM) for different needle's closing laws are compared with the results of measurements. The following results of measurements and corresponding numerical simulations are presented:

1. Emergency shut-down of turbine unit A1 from initial power P_0 = 37 MW (Test A1P37MW is Test A),
2. Simultaneous load rejection under governor control of turbine units A1 and A2 from initial power of P_0 = 42 MW each (Test A1&A2P42MW is Test B),

In addition, speed change during stop procedure of the turbine unit A1 is included too. The main initial parameters for the two test cases are presented in Tables 3, 4 and 5. The flow in penstock *I* is turbulent with a large Reynolds number (Re_I). Pressure wave speeds for all tests are as follows, a_T = 1354 m/s, a_I = 1148 m/s, a_{II} = 1123 m/s and a_{III} = 1152 m/s.

4.1 Comparison of Numerical and Measured Head at the Turbine Inlet

Transient head and discharge for the power plant flow-passage system were computed using a staggered grid MOC code. Basic time step was Δt = 0.04 s. Computed and measured results are shown in Figs. 4, 5 and 6.

Computed and measured heads at the turbine inlet for emergency shut-down of the turbine unit A1 are shown in Fig. 4 (Test A). The calculated and the measured total needle closing times are the same (t_c = 56.1 s see Fig. 4a). The closing time is much larger than the water hammer reflection time of $2L_I/a_I$ = 3.84 s. The maximum measured head of 557.7 m occurs at the end of the nozzle closure period with the head rise of 24.5 m. The maximum calculated heads match the measured i.e. 557.5 m obtained by QSF (see Fig. 4b) and 557.8 m obtained by CBM (see Fig. 4c). The calculated and measured heads are much lower than the maximum permissible head of 602 m. The numerical results using two-speed needle stroke [17] show very good agreement with the measured results during the nozzle closure period. After this, a slight phase shift of numerical results is evident from the third pressure pulse but with good attenuation at all times. Friction losses are described slightly better by the CBM model during the decay period of transient process. It is evident that the Perućica flow-passage system is not an unsteady friction dominant system during water hammer events. Comparisons between numerical results using two-speed (theoretical) needle stroke (TNS) and actual (measured) needle stroke (ANS) (see Fig. 4d) show that TNS model adequately simulates water hammer events during emergency shut-down of the turbine unit.

Table 3. *Initial discharges through tunnel (Q_T) and penstocks (Q_I, Q_{II}, Q_{III})*

Test	Q_I (m^3/s)	$Re_I \times 10^6$	Q_{II} (m^3/s)	Q_{III} (m^3/s)	Q_T (m^3/s)
A	8.45	5.5	0	19.7	28.15
B	18.2	11.8	0	5.7	23.9

Table 4. *Steady friction factors (f_0) and momentum correction factors (β) for all tests*

Test	Penstock *I*		Penstock *II*		Penstock *III*		Tunnel	
	f_0	β	f_0	β	f_0	β	f_0	β
A	0.0107	1.0106	0.0118	1.0115	0.0155	1.0151	0.0146	1.0143
B	0.0104	1.0102	0.0118	1.0115	0.0156	1.0153	0.0146	1.0143

Table 5. *Intake level (z_R), needle closing time (t_c), initial opening of the nozzle (s_0) and jet deflector operating time (t_{def})*

Test	z_R (m)	t_c (s)	s_0 (mm)	t_{def} (s)
A	605.8	56.1	117	1.6
B	604.8	85.3	146	2.0

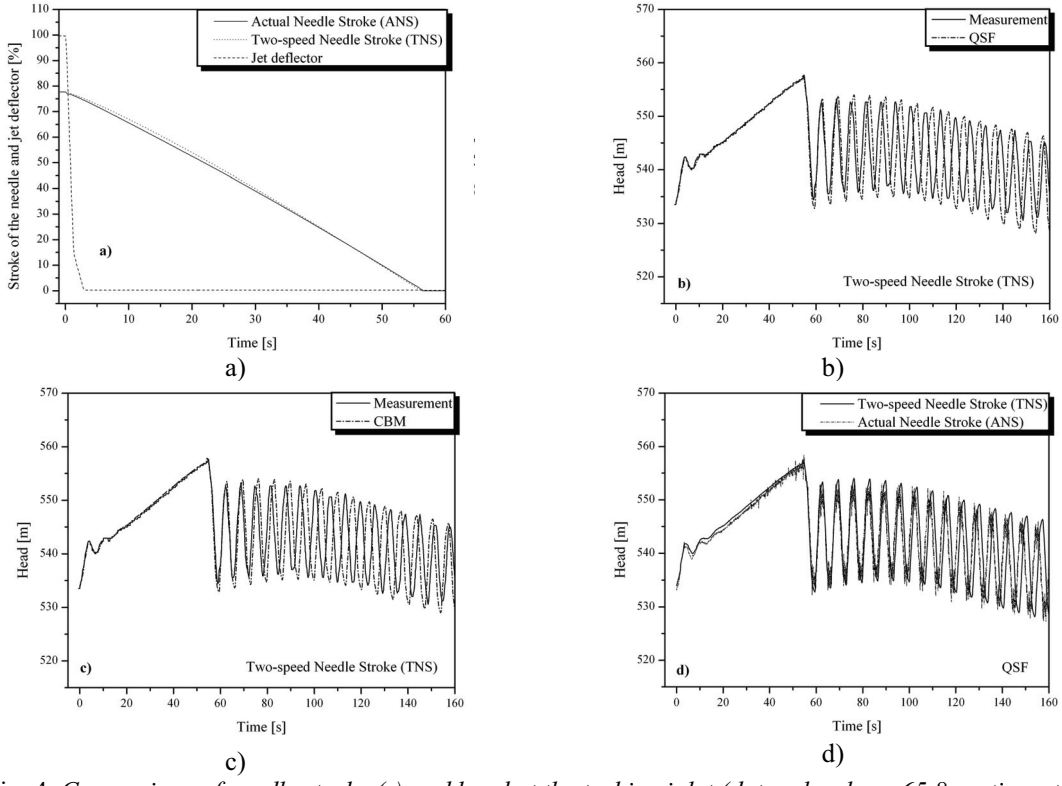

Fig. 4. *Comparison of needle stroke (s) and head at the turbine inlet (datum level z = 65.8 m; time step Δt=0.04 s). Emergency shut-down of A1 from P_0 = 37 MW (Test A).*

The computed and measured heads at the turbine inlet for simultaneous load rejection under governor control of turbine units A1 and A2 are compared in Fig. 5. Test B produces maximum measured head of 573.9 m at the end of the nozzle closure period with head rise of 57.2 m. For all numerical calculations the ANS model was employed. The maximum calculated head obtained by QSF is 574.0 m (see Fig. 5b) and by CBM is 574.4 (see Fig. 5c). The needle closure process to its speed-no load position (3.25%) is governed by the turbine control system and is followed by gradual adjustment of the jet deflector to its appropriate position (see Fig. 5a). Up to this time all numerical models show reasonable agreement with results of measurement. The maximum calculated heads are well below the maximum permissible head of 602 m. Numerical models produce practically the same results after the closure period (see Fig. 5d).

Finally, it should be noted that the used staggered grid MOC code was thoroughly tested for convergence and stability in [17] and [20]. The code proved to be numerically robust.

4.2 Comparison of Calculated and Measured Turbine Rotational Speed

Turbine rotational speed change during emergency shut-down of turbine unit A1 (Test A) and during simultaneous load rejection under governor control of turbine units A1 and A2 (Test B) was calculated using appropriate solution method of the dynamic equation of the unit rotating parts (Eq. (12)). The instantaneous head and discharge through the nozzle during these transient regimes were previously calculated by the MOC (see Section 4.1). Fig. 6 shows comparison between calculated and measured rotational speed change for both case studies.

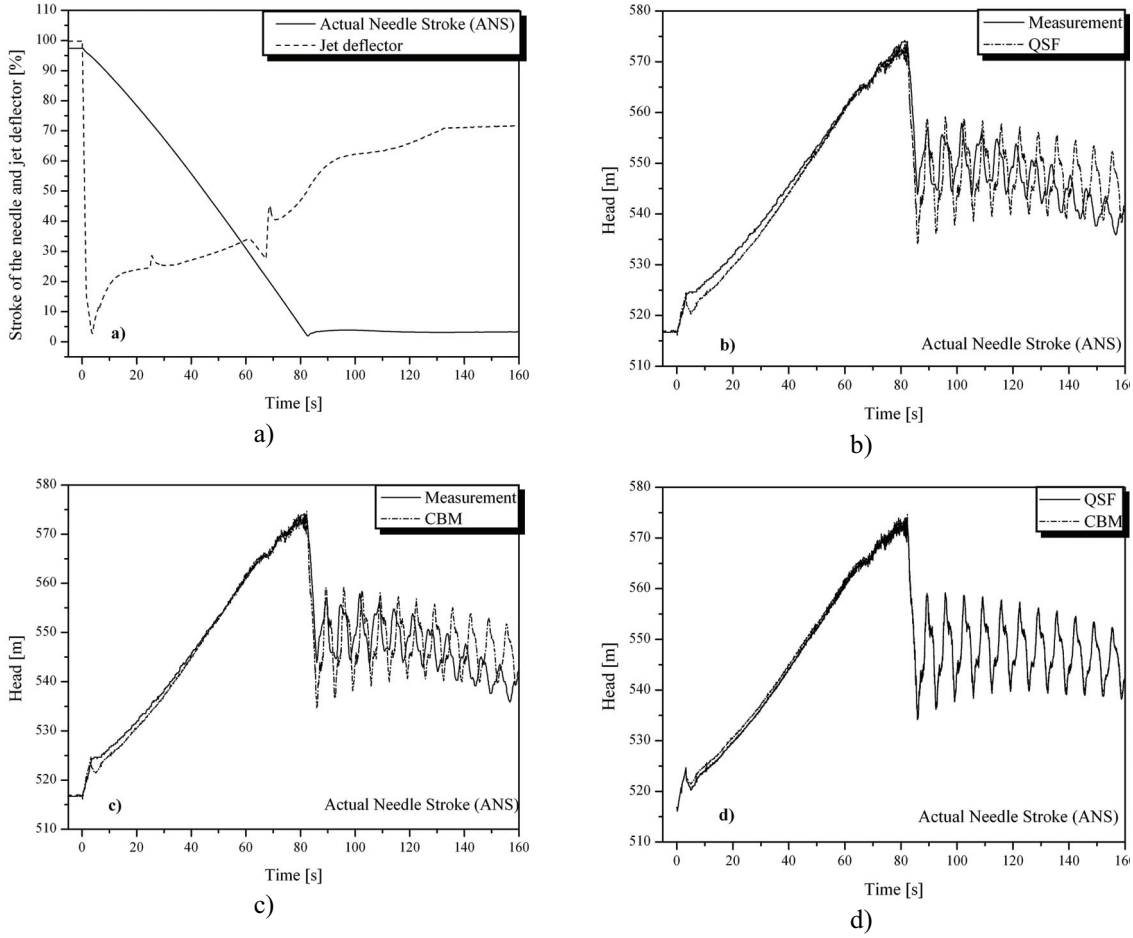

Fig. 5. *Comparison of needle stroke (s) and head at the turbine inlet (datum level z = 65.8 m; time step Δt=0.04 s). Simultaneous load rejection under governor control of A1 and A2 from P_0 = 42 MW (Test B).*

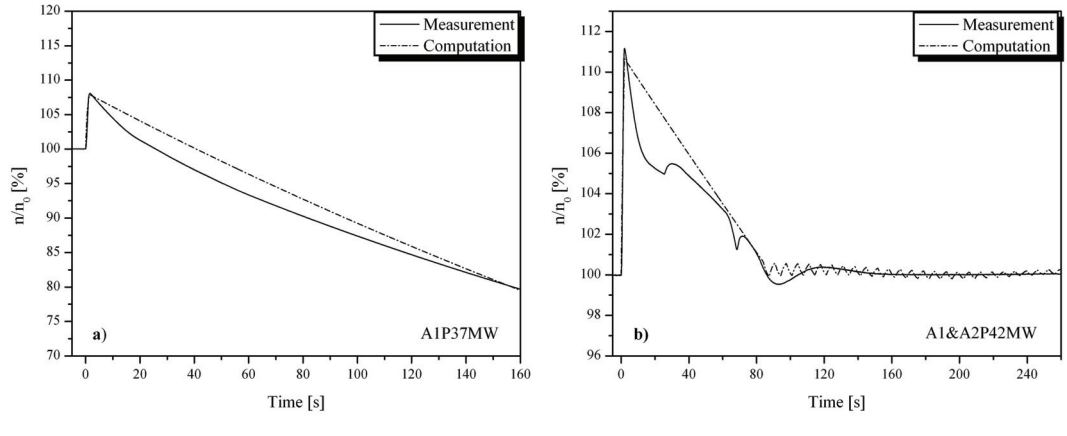

Fig. 6. *Rotational speed change (n_0 = 375 min^{-1}) during emergency shut-down of A1 from P_0 = 37 MW (Test A) and simultaneous load rejection under governor control of A1 and A2 from P_0 = 42 MW (Test B).*

The maximum measured turbine speed rise for Test A of 8.1% occurs at time $t = t_{def}$. The maximum calculated turbine speed rise of 8.1% perfectly agrees with measured one (see Fig. 6a). After the jet deflector deflects all the water into the tailrace, the turbine wheel is not affected by hydraulic torque and the turbine speed decrease is influenced by dissipation torques. During this period the calculated turbine speed reasonably agrees with measured one. There is a very good agreement between the maximum measured and computed turbine speed rise for Test B of 11.2% and 11.1%, respectively (see Fig. 6b). There are some discrepancies in the phase of speed decrease due to complex flow behaviour in the turbine housing. The ventilation losses are dependent on fluid density inside the turbine housing. The fluid is basically air but it does contain a mist of water and this will increase complexity of flow behaviour. In both investigated cases the maximum turbine speed rise is well below the permissible speed rise of 25%.

Turbine rotational speed change during stop procedure of the turbine unit A1 from speed no-load conditions using hydraulic brake is shown in Fig. 7. There is a good agreement between measured and computed results. The process of turbine stopping lasts for about 560 s.

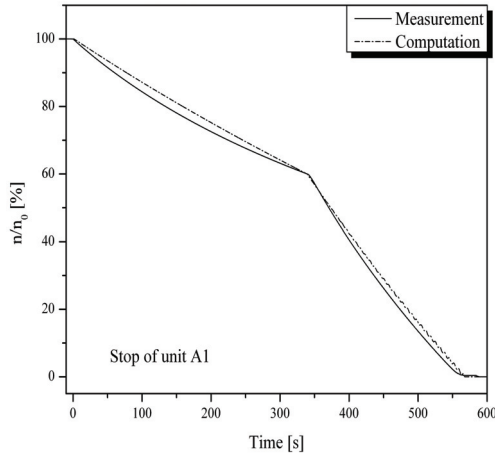

Fig. 7. *Stop of unit A1 from speed no-load conditions using hydraulic brake (n_0 = 375 min^{-1})*

5 CONCLUSIONS

Comparisons of computed and experimental results given for quasi-steady friction model (QSF) and convolution based unsteady friction model (CBM) for different needle closing laws are made for turbine load rejection cases (load rejection under governor control, emergency shut-down). Turbine unit stop procedure is also investigated. Numerical results obtained by QSF and CBM models are practically the same because the investigated case studies represent slow varying transients in long pipelines. The effect of unsteady friction for these cases is negligible. Numerical results obtained by the model with two-speed needle stroke (TNS) agree well with the results of measurement and with numerical results obtained by the model that considers actual (measured) needle stroke (ANS) for the case of emergency shut-down of the turbine unit. The TNS model captures natural damping effect in the needle hydraulic servomotor close to its fully closed position and successfully simulates real nature of water hammer events during emergency shut-down of the turbine unit. For the case of load rejection under governor control the TNS model is not employed because the speed no-load needle position is larger than the needle position when the second closure step begins. A novel model of Pelton turbine rotational speed change is used for calculating transient rotational speed. There is a reasonable agreement between the calculated and measured results for all the investigated cases.

6 REFERENCES

[1] Pejović, S., Boldy, A.P., Obradović, D. (1987), Guidelines to hydraulic transient analysis, *Gower Technical Press Ltd.*, Aldershot, UK, ISBN 0-291-39723-9.

[2] Krivchenko, G.I., Arshenevskij, N.N., Kvjatovskaja, E.V., Klabukov, V.M. (1975), Hydraulic transients in hydro-electric power plants, *Energija,* Moscow, Russia (in Russian).

[3] Wylie, E.B., Streeter, V.L. (1993), Fluid transients in systems, *Prentice Hall,* Englewood Cliffs, USA, ISBN 0-13-322173-3.

[4] Chaudhry, M.H. (1987), Applied hydraulic transients, *Van Nostrand Reinhold Company,* New York, USA, ISBN 0-442-21514-2.

[5] Evangelisti, G., Boari, M., Guerrini, P., Rossi, R. (1973 & 1974), Some applications of waterhammer analysis by the method of characteristics, *L'Energia Elettrica*, 50(1), 1-12 & 51(6), 309-324.

[6] Fasol, K.H. (1964), Consideration of dynamic characteristics of Pelton turbine nozzles in water hammer analysis, *ÖZE - Österreichische Zeitschrift für Elektrizitätwirtschaft*, 17(8), p. 453-456 (in German).

[7] Zielke, W. (1968), Frequency-dependent friction in transient pipe flow, *Journal of Basic Engineering*, ASME, 90(1), 109-115.

[8] Bergant, A., Simpson, A.R., Vítkovský, J. (2001). Developments in unsteady pipe flow friction modeling, *Journal of Hydraulic Research*, IAHR, 39(3), p. 249-257.

[9] Vardy, A.E. (1980), Unsteady flows: Fact and friction. *Third International Conference on Pressure Surges, BHRA*, Canterbury, UK, p. 15-26.

[10] Haaland, S.E. (1983). Simple and explicit formulas for the friction factor in turbulent pipe flow, *Journal of Fluids Engineering*, ASME, 105(3), p. 89-90.

[11] Vítkovský, J., Stephens, M., Bergant, A., Lambert, M., Simpson, A. (2004), Efficient and accurate calculation of Zielke and Vardy-Brown unsteady friction in pipe transients, *Proceedings of the 9th International Conference on Pressure Surges, BHR Group*, Chester, UK, 15 pp.

[12] Vardy, A.E., Brown, J.M.B. (2003), Transient turbulent friction in smooth pipe flows, *Journal of Sound and Vibration*, 259(5), p. 1011-1036.

[13] Vardy, A.E., Brown, J.M.B. (2004), Transient turbulent friction in fully rough pipe flows, *Journal of Sound and Vibration*, 270(1-2), p. 233-257.

[14] Bergant, A., Karadžić, U., Vítkovský, J., Vušanović, I., Simpson, A.R. (2005), A discrete gas-cavity model that considers the frictional effects of unsteady pipe flow, *Strojniški Vestnik – Journal of Mechanical Engineering*, 51(11), p. 692-710.

[15] Chen, C.L. (1992), Momentum and energy coefficients based on power-law velocity profile, *Journal of Hydraulic Engineering*, ASCE, 118(11), p. 1571-1584.

[16] Benišek, M. (1998), Hydraulic turbines, *Faculty of Mechanical Engineering*, Belgrade, Serbia, (in Serbian), ISBN 86-7083-323-9.

[17] Karadžić, U., Bergant, A., Vukoslavčević, P. (2008), Parameters affecting water hammer in a high-head hydropower plant with Pelton turbines. *Proceedings of the 10th International Conference on Presure Surges, BHR Group*, Edinburgh, UK, p. 351-364.

[18] Nechleba, M. (1957), Hydraulic turbines – their design and equipment, *Artia*, Prague, Czech Republic.

[19] Zhang, Zh., Müller, J. (2007), Efficiency and runaway characteristics of a Pelton turbine. *Hydro 2007*, Granada, Spain.

[20] Karadžić, U. (2008), Modelling of complex boundary conditions for transients in hydraulic systems, PhD Thesis, *Faculty of Mechanical Engineering*, University of Montenegro, Podgorica, Montenegro (in Montenegrian).

[21] Thake, J. (2000). The micro-hydro Pelton turbine manual. *ITDG Publishing*, London, UK, ISBN 1-85339-460-2.

[22] Bajcar, T., Širok, B., Eberlinc, M. (2009), Quantification of flow kinematics using computer-aided visualization, *Strojniški Vestnik – Journal of Mechanical Engineering*, 55(4), p. 215-223.

[23] Spiegel, M.R. (1968), Handbook of mathematical formulas. *Rensselaer Polytechnic Institute*, Troy, New York, USA, ISBN 0-07-060224-7.

[24] Edelj, J.U. (1963), *Impulse water turbines – theory, research, analysis*, Mashgiz, Moscow, Russia (in Russian).

[25] Rek, Z., Bergant, A., Röthl, M., Rodič, P., Žun, I. (2008), Analysis of hydraulic characteristics of guard-gate for hydropower plant, *Strojniški Vestnik – Journal of Mechanical Engineering*, 54(1), p. 3-10.